1-1-2013

Tuning of the transverse magneto-optical Kerr effect in magneto-plasmonic crystals

Martin Pohl

L. E. Kreilkamp

Vladimir I. Belotelov

Ilya A. Akimov

A N. Kalish

See next page for additional authors

10.1088/1367-2630/15/7/075024

Pohl, M., Kreilkamp, L., Belotelov, V., Akimov, I., Kalish, A., Khokhlov, N., Yallapragada, V., Gopal, A., Nur E Alam, M. , Vasiliev, M. , Yakovlev, D., Alameh, K. , Zvezdin, A., & Bayer, M. (2013). Tuning of the transverse magneto-optical Kerr effect in magneto-plasmonic crystals. New Journal Of Physics, 15, Article 075024. Available here

Tuning of the transverse magneto-optical Kerr effect in magneto-plasmonic crystals

2013 New J. Phys. 15 075024

(http://iopscience.iop.org/1367-2630/15/7/075024)

New Journal of Physics
The open access journal for physics

Tuning of the transverse magneto-optical Kerr effect in magneto-plasmonic crystals

M Pohl[1], L E Kreilkamp[1], V I Belotelov[2,3,4,9], I A Akimov[1,5,9], A N Kalish[2,3,4], N E Khokhlov[2,3], V J Yallapragada[6], A V Gopal[6], M Nur-E-Alam[7], M Vasiliev[7], D R Yakovlev[1,5], K Alameh[7], A K Zvezdin[3,4,8] and M Bayer[1]

[1] Experimentelle Physik 2, Technische Universität Dortmund, D-44221 Dortmund, Germany
[2] Lomonosov Moscow State University, 119991 Moscow, Russia
[3] Russian Quantum Center, 143025 Moscow, Russia
[4] Prokhorov General Physics Institute, Russian Academy of Sciences, 119991 Moscow, Russia
[5] Ioffe Physical-Technical Institute, Russian Academy of Sciences, 194021 Saint Petersburg, Russia
[6] Tata Institute of Fundamental Research, 400005 Mumbai, India
[7] Electron Science Research Institute, Edith Cowan University, 6027 Joondalup, WA, Australia
[8] Moscow Institute of Physics and Technology (State University), 141700, Dolgoprudny, Russia
E-mail: belotelov@physics.msu.ru and ilja.akimov@tu-dortmund.de

New Journal of Physics **15** (2013) 075024 (14pp)
Received 22 April 2013
Published 26 July 2013
Online at http://www.njp.org/
doi:10.1088/1367-2630/15/7/075024

Abstract. The spectral properties of the transverse magneto-optical Kerr effect (TMOKE) in periodic metal–dielectric hybrid structures are studied, in particular with respect to the achievable magnitude. It is shown that the TMOKE is sensitive to the magneto-optical activity of the bismuth-substituted rare-earth iron garnet, which is used as a dielectric material in the investigated structures. For samples with larger Bi substitution level and, consequently, larger gyration

[9] Authors to whom any correspondence should be addressed.

constant, the magnitude of the TMOKE increases and reaches 13% in the case of a $Bi_{1.8}Lu_{1.2}Fe_{3.6}Al_{1.4}O_{12}$ magnetic film. Further, it is demonstrated that the TMOKE vanishes at the high-symmetry points of the Brillouin zone (at the Γ and X points). The main enhancement of the TMOKE takes place near the resonances of the surface plasmon polaritons (SPPs) at the metal/magnetic–dielectric interface. However, near the degenerate resonances of the SPPs at the air/metal and metal/magnetic–dielectric interfaces the TMOKE is increased by the air/metal SPPs as well. This phenomenon is explained in terms of a coupled oscillator model.

Contents

1. Introduction

The amplitude, phase and polarization of light passing through a magnetized medium can be modulated by the medium's magnetization [1, 2]. On the other hand, it was demonstrated recently that one can manipulate the medium's magnetization optically on sub-nanosecond time scales [3]. This makes magneto-optics quite promising as a tool for controlling light in modern optical devices.

Magneto-optical effects that provide modulation of light intensity are represented by the transverse magneto-optical Kerr effect (TMOKE). The TMOKE is observed when obliquely incident light illuminates a magnetic film magnetized in-plane and perpendicular to the incidence plane. The TMOKE is characterized by the parameter δ, which represents the relative change in the intensity I of the light reflected by the medium when its magnetization M is reversed:

$$\delta = \frac{I(\boldsymbol{M}) - I(-\boldsymbol{M})}{I(0)}. \tag{1}$$

The TMOKE allows one to investigate the magnetic properties of a medium and can be utilized in magneto-optical data storage [2, 4]. The relative change in the reflected light intensity due to the TMOKE in ferromagnets such as nickel or cobalt is of the order of 10^{-3}, limiting TMOKE applicability [2]. Recently, several concepts were proposed to resonantly increase the TMOKE [5–10]. Specifically, these concepts involve surface plasmon polaritons (SPPs)—coupled oscillations of the electromagnetic field and the electron plasma in a metal,

which propagate along a metal/dielectric interface [11]. The combination of plasmonics and magneto-optics looks mutually beneficial. On the one hand, the magnetic field is an efficient tool to control SPPs [12, 13], and on the other hand SPPs can be utilized to enhance magneto-optical effects [14–30].

Early papers on the interplay between SPPs and magneto-optics addressed SPPs propagating along the smooth surface of a ferromagnetic film [31, 32] or along a smooth semiconductor surface in an external transverse magnetic field [33, 34]. In that case, the magnetic field modifies the SPP wave vector, but leaves the polarization of the SPP unchanged.

Periodic perforation of metal layers provides Fano resonances in transmission or reflection spectra due to SPP excitation [35], which are usually referred to as Wood anomalies [36]. The appearance of Fano resonances in the spectra of the perforated metallic ferromagnets gives a several times enhancement of the TMOKE [5, 21, 37]. Owing to a periodicity comparable to the SPP wavelength, such structures can be referred to as magneto-plasmonic crystals (MPCs). However, ferromagnetic metals introduce optical losses that are too large to be acceptable in practical applications. Reduction of optical losses was achieved in bimetallic systems of noble and ferromagnetic metals, either smooth or perforated [6, 7, 22, 23, 38–41]. The SPPs can propagate relatively long distances along the noble metal/air interface and they enhance the TMOKE, which takes place at the ferromagnetic surface. This concept provided further enhancement of the TMOKE by several times. In [13], a Mach–Zehnder interferometer was used to demonstrate that minute magneto-optical phase shifts of the SPPs in a gold/cobalt bilayer structure could be detected. Coexisting SPPs and localized surface plasmons were studied in Au/Co/Au trilayer films covered by Au nanodiscs with a SiO_2 spacer [7].

Another approach demonstrated recently by Belotelov *et al* [8, 10, 15] is to substitute the ferromagnetic metal by a noble metal layer with low optical absorption and to introduce a magnetic–dielectric layer into the MPC. It allows the SPPs to propagate with relatively low losses right at the magnetized interface without any spacing which makes the TMOKE even larger [8]. This enhancement is mediated by the SPPs at the metal/magnetic–dielectric interface leading to Fano resonances in the transmittance and reflectance spectra that are sensitive to a transverse magnetic field.

Here, we concentrate our studies on several features of the TMOKE in MPCs of similar structure consisting of a gold grating on top of a magnetic layer of bismuth-substituted rare-earth iron garnet on a gadolinium gallium garnet (GGG) substrate. In particular, we compare the TMOKE signal strength in the MPCs comprising magnetic layers of different magneto-optical activity. Further, we investigate the TMOKE dispersion in the vicinity of some specific points of the first Brillouin zone. These points include the center and the edges of the Brillouin zone and points where the dispersion curves of the SPPs propagating along two surfaces of the metal grating intersect. Finally, we compare TMOKE data measured in reflection and transmission geometries.

2. Experimental technique

Each MPC sample under study in this paper consists of a nanometer-sized gold grating on top of a bismuth iron garnet (BIG) magnetic film of few micrometers thickness deposited onto a GGG substrate. Apart from minor differences in the grating parameters and fabrication techniques, the major difference between the samples lies in the relative amount of bismuth ions (per stoichiometric formula unit) inside the magnetic films, which influences the magneto-optical

Table 1. Overview of the magneto-optical film compositions, fabrication techniques and magneto-optical properties along with gold-grating geometrical parameters of the investigated MPC samples. d is the gold grating period, r is the slit width of the gold grating, h_m is the thickness of the gold grating and h_d is the magnetic film thickness. Diagonal (ϵ) and non-diagonal (gyration g) terms of the permittivity tensor are given at photon energy 1.55 eV.

Sample	Chemical composition	Fabrication technique	ϵ g	Geometrical parameters (nm)
1	$Bi_{1.8}Lu_{1.2}Fe_{3.6}Al_{1.4}O_{12}$	RF magnetron sputtering	$\epsilon = 5.29 + 0.017i$ $g = 0.0085$ $\epsilon = 5.18 + 0.013i$	$d = 605$ $r = 160$ $h_m = 125$ $h_d = 905$ $d = 505$
2	$(BiSmTm)_3(FeGa)_5O_{12}$	Liquid phase epitaxy	$g = 0.0051$ $\epsilon = 4.98 + 0.005i$	$r = 85$ $h_m = 100$ $h_d = 5095$ $d = 595$
3	$Bi_{0.4}(YGdSmCa)_{2.6}(FeGeSi)_5O_{12}$	Liquid phase epitaxy	$g = 0.0017$	$r = 110$ $h_m = 120$ $h_d = 2500$

properties of the garnets [42]. The bismuth substitution level can be seen to be decreasing from sample 1 to 3 in table 1. A sketch of the principle design is given in figure 1(a).

For the magneto-optical measurements, we used a tungsten halogen lamp with stability better than 0.1%. The light was imaged onto a 100 μm pinhole in order to establish a point source of white light. The transmitted light was then collimated with an achromatic lens (focal distance of $f_1 = 150$ or alternatively 300 mm) and focused onto the sample using a second achromatic lens with a focal distance of $f_2 \leqslant f_1$. A diaphragm has been used between the doublets in order to reduce the maximum angle of the incident light cone to below 1°. The light was focused on the sample into spots with diameters from 50 to 300 μm, depending on the dimensions of the grating patterns. To perform measurements at different angles of light incidence, the sample was mounted on a rotation stage. The zero-order transmission and reflection signals were spectrally dispersed with a single monochromator (linear dispersion 4.8 nm mm^{-1} at 900 nm) and detected with a charge-coupled device camera. The overall spectral resolution was about 0.5 nm. The p-plane linear polarization of the light was established by a polarizer in the excitation path, i.e. before the sample. Magnetic fields up to $B = 180$ mT were applied in transverse geometry using a water cooled electromagnet. During measurement the sample was kept at room temperature.

Figure 1(b) represents a typical transmission spectrum, which exhibits a characteristic Fano feature corresponding to an SPP resonance. The transmitted or reflected light intensities $I(E)$ near a Fano resonance are given by the sum of a resonant I_r and a non-resonant I_{nr} contribution:

$$I(E) = I_r(E) + I_{nr}, \tag{2}$$

where $E = \hbar\omega$ is the photon energy. The resonant channel is due to plasmon excitation, while the non-resonant one represents direct transmission or reflection. The resonantly scattered wave

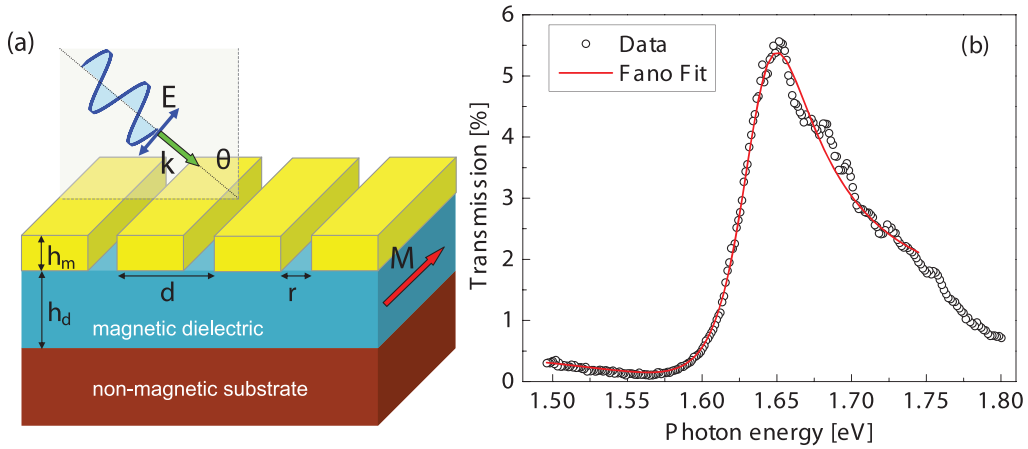

Figure 1. (a) The magneto-plasmonic heterostructures consist of a gold grating on top of a planar ferromagnetic–dielectric (bismuth iron garnet film) grown on a non-magnetic substrate (gadolinium gallium garnet). The parameters of the gold film for the three samples are listed in table 1. The sketch shows the TMOKE geometry, i.e. **M** is perpendicular to the plane of incidence and is in the sample plane. Incident light is p-polarized, i.e. its electric field **E** lies in the plane of incidence. (b) An exemplary Fano feature in the transmission spectrum (circles) of sample 1 for $\theta = 0^\circ$ incidence. The data has been fitted with equation (3) (solid curve), which gives the resonance position and width of $\hbar\omega_i = 1.64\,\mathrm{eV}$ and $\Gamma_i = 0.06\,\mathrm{eV}$, respectively (cf figure 2(a)).

experiences a phase shift of π across the resonance energy, resulting in constructive and destructive interference with the non-resonantly scattered light and thus the characteristic asymmetric lineshape of the features in the transmission and reflection spectra (see figure 1(b)) [35].

In order to determine the position of the SPP resonances in the transmission and reflection spectra, they have been approximated by a sum of up to three Fano shapes located at different energies:

$$I = \sum_{i=1}^{3} A_i (1 + E_i Q_i)^2 / (1 + E_i^2) + D \tag{3}$$

with $E_i = (\omega - \omega_i)/(\Gamma_i/2)$ and $D = D_0 + D_{\mathrm{lin}}\omega$. Here, A_i, ω_i and Γ_i are the amplitude, position and width of resonance i, while Q_i is a parameter describing its degree of asymmetry, which depends on the ratio of the intensities of the two interfering resonant and non-resonant channels. All other contributions with weak spectral dependence are taken into account by D. The number of Fano resonances in equation (3) corresponds to the maximum of three branches of SPP dispersions that are simultaneously present in the energy range of the transmission/reflection spectra (see figure 4(a)).

For TMOKE measurements the magnetic field was applied along the MPC slits and perpendicular to the incidence plane (see figure 1(a)). The spectral dependence of δ has been evaluated using equation (1) where the transmission or reflection spectra measured for different directions of the magnetic field B, i.e. of the magnetization M, have been used.

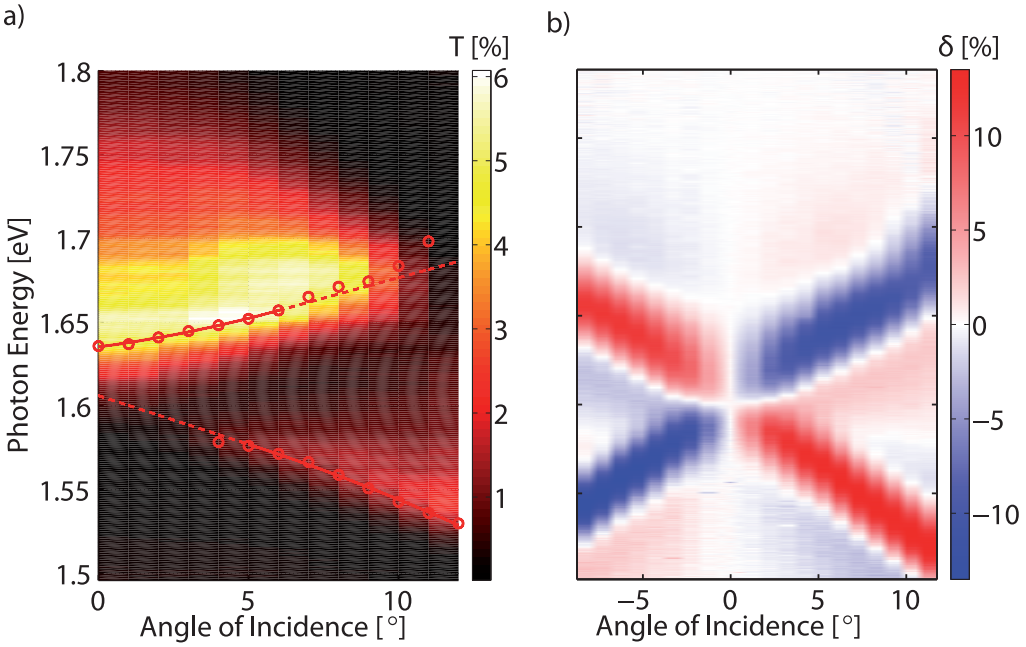

Figure 2. (a) Measured angle dependence of the transmitted light spectrum of sample 1 between $\theta = 0^\circ$ and 12° in steps of 1° without applied magnetic field. Open circles show the position of the Fano resonances. The dashed lines are meant as guide to the eyes. (b) Measured angle dependence of the TMOKE in transmission on sample 1 with an applied external magnetic field of $B = 80\,\mathrm{mT}$. For symmetry reasons the effect vanishes for normal incidence and reverses sign when the incidence angle is reversed. For angles $\theta \geqslant 4^\circ$ a remarkably high value of $\delta = 13\%$ is reached.

3. Dependence of the transverse magneto-optical Kerr effect (TMOKE) magnitude on the bismuth substitution level

Figure 2(a) shows the transmission spectrum of sample 1 for incidence angles between $\theta = 0^\circ$ and 12°.

The transmitted intensity normalized to the spectral distribution of the illuminating white light source is color coded and given in per cent. The position of the resonances corresponding to SPPs excited on the gold/magnetic–dielectric interface by the ± 2nd diffraction orders are indicated by open circles. These data points were obtained by fitting the individual transmission features by the Fano formula (equation (3)). The lines serve as guides to the eye to illustrate the energy dispersion of the two modes.

The TMOKE signal of this sample is depicted in figure 2(b) for both positive and negative incidence angles θ. A comparison with figure 2(a) shows that the positions of the TMOKE resonances follow closely the positions of the plasmonic resonances. This is because the observed change in transmission upon application of an external magnetic field, given by the parameter δ, is induced by a shift of the plasmonic resonance. The magnetization M of the magnetic film leads to a change of the wave number k of the plasmonic mode. In the

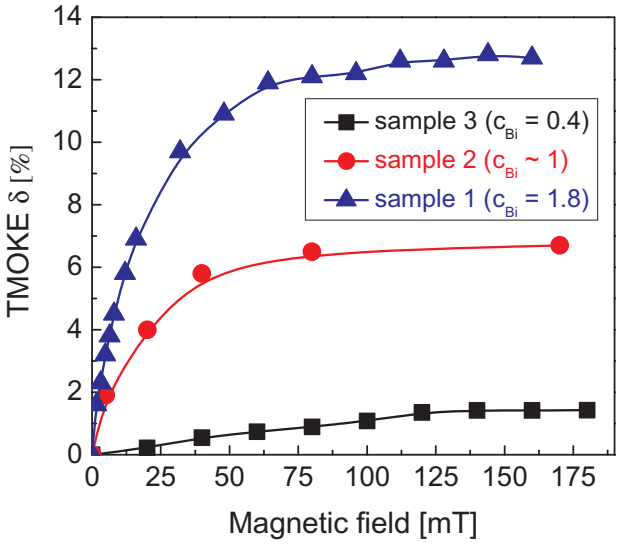

Figure 3. Magnetic field dependence of the TMOKE in transmission measured under oblique incidence for three different samples with varying bismuth content c_{Bi}. The amplitude of a particularly strong TMOKE peak for each sample is shown. The maximum attainable value of the effect rises with increasing bismuth content. The solid lines are used to guide the eye.

case of a smooth metal/magnetic dielectric, it can be written as

$$k = k_0(1 + \alpha g), \tag{4}$$

where k_0 is the wavenumber for $M = 0$, α is a frequency-dependent coefficient and $g \propto M$ is the component of the gyration vector perpendicular to k [8]. Owing to the energy dispersion $E(k_0)$ of SPP, this translates into a shift of the resonance energy of the SPP and consequently of the transmission maximum. It follows from the structure symmetry that a reversal of the incidence angle is equivalent to the reversal of M at constant angle of incidence. In accordance with equation (4) the TMOKE is odd in M. Therefore, it is odd in the incidence angle as well. Symmetry reasons enforce that the TMOKE is only present for oblique incidence. Compared to earlier measurements on a similar MPC [8], the observed maximum TMOKE is enhanced by roughly one order of magnitude.

In order to illustrate the origin of the higher TMOKE values, we compare its magnetic field dependence in samples with different bismuth substitution levels. Figure 3 shows the dependence of the maximum achievable TMOKE amplitude in dependence of the applied external magnetic field B for samples 1–3 (see table 1).

All three curves show a progression characteristic for the magnetization curve in ferromagnetic BIG materials: for low-field strengths, there is a linear dependence of the effect on the applied magnetic field since the magnetic domains, originally oriented along the easy axis, are turned along the external field. Further increase of the magnetic field leads to a saturation of the magnetization M and thus of the observed TMOKE. The saturation values for the effect grow with the bismuth substitution level. Sample 3 has a small amount of bismuth and therefore its magneto-optical activity is weak. As a result the TMOKE is limited to a maximum value of 1.5% in this sample. For sample 2, whose bismuth substitution level is $c_{\mathrm{Bi}} \approx 1$, the magnetic

field dependence is given by the red dots. For this sample the saturation value of the TMOKE amplitude lies around 7%. The largest TMOKE amplitude is measured for sample 1 amounting to 13% under saturated magnetization.

The experimental data clearly demonstrate that the magnitude of the TMOKE induced by a magnetic medium is dependent on its gyration g, i.e. on its magneto-optical activity, which can be tailored by optimal choice of chemical composition. The other important aspect is the value of the saturating magnetic field. It is closely related to the magnetic anisotropy of the magnetic film and depends on the composition as well as on the thickness. The magnetic films of samples 2 and 3 have a uniaxial magnetic anisotropy perpendicular to their surfaces, while the magnetic film of sample 1 has a uniaxial magnetic anisotropy that forms a small angle with the sample surface. Because of the differences in their composition their saturating magnetic fields vary. Sample 2 has the smallest one of about 60 mT.

4. TMOKE related to surface plasmon polaritons from different interfaces: spectral tunability

While the achieved TMOKE magnitude values are already on the scale that would be manageable in practical device applications, further potential of MPCs lies in the interaction of both of its SPP modes, which are provided owing to the two interfaces of the noble metal. Here, it is interesting to investigate the effect of possible coupling between SPPs from different interfaces on the TMOKE. This coupling should take place in the regions of intersecting SPP dispersions. Here, we concentrate on sample 2 with moderate bismuth substitution level whose plasmon dispersions show the desired intersections within the first Brillouin zone (1.BZ). Transmission and reflection spectra have been measured across a wide range of incidence angles and are summarized in figure 4. The fitting results obtained using equation (3) are shown in figure 4(a) as full (reflection) or open (transmission) circles for the Au/BIG SPPs (red) and the Au/air SPPs (black) for different angles of the 1.BZ. The results are in good agreement with a Drude model calculation of the SPP dispersions in the empty lattice approximation, which is shown in figure 4(b). Exemplary spectra as well as the corresponding Fano fits can be found in figures 4(c)–(e). However, a closer look reveals a deviation from the model at photon energies around 1.4 eV, where the experiment reveals an anti-crossing and a subsequent splitting of the branches of the SPP dispersions at the intersection, which is characteristic of strong coupling.

Corresponding TMOKE measurements are shown in figures 5(a) and (b) for angles close to the center and the edge of the 1.BZ.

The strength of the externally applied magnetic field was held constant at $B = 170$ mT. Remarkably, the TMOKE amplitude vanishes at both symmetry points, i.e. at $\theta = 0^\circ$ and 61°. At these points, two SPPs are excited simultaneously having opposite wavenumbers k. Consequently, the TMOKE for each of the SPPs differs in sign and cancels to zero (see also [8]). The shift of the signals at angles larger than zero, indicated by the red dashed lines, follows the Au/BIG SPP dispersion shown in figure 4(a). Additionally, at the intersection of both SPPs, figure 5(b) clearly shows TMOKE features that shift according to the Au/air SPP (black dashed line), whose resonances are expected to be independent of the magnetization of the dielectric.

The presence of the effect at the air/metal SPP for photon energies in the vicinity of the metal/magnetic–dielectric SPP excitation can be understood in terms of a coupled oscillator model. In the framework of this model, the SPPs at the two interfaces of the metallic grating are considered as two oscillators with their coupling coming from the finiteness of the grating

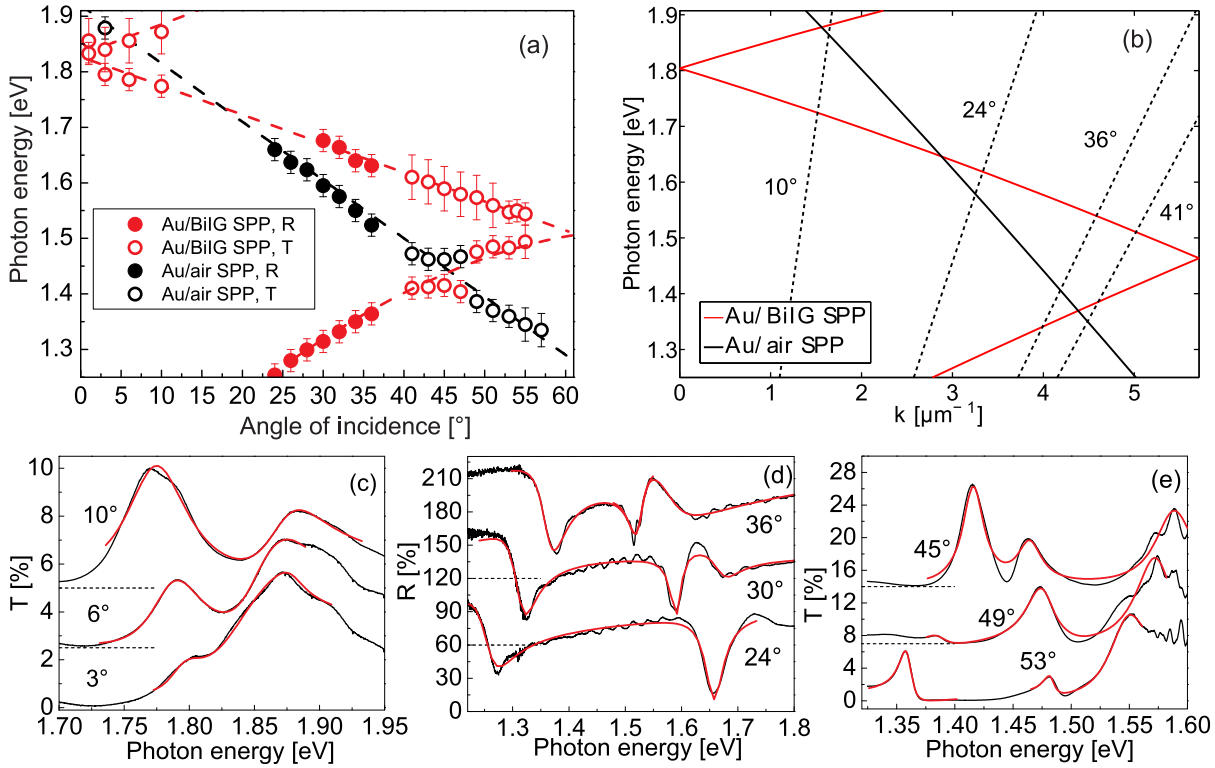

Figure 4. Dispersion relations of the SPPs at the Au/BIG (red) and Au/air (black) interfaces of sample 2 within the first Brillouin zone (a) as obtained by fitting equation (3) to the SPP features in the transmission (see figures 4(c) and (e)) and reflection (see figure 4(d)) spectra and (b) by means of a Drude model calculation for a grating period d and the dielectric constant of the magnetic film $\epsilon_d = 4.5$. The intersection of the SPP dispersion curves leads to a splitting, i.e. anti-crossing around an incidence angle of 40° in figure 4(a). Selected transmittance and reflectance spectra are shown in figures 4(c) and (e), as well as figure 4(d), which also give the results of the Fano fits (red curves). The spectra are shifted for clarity. The dashed lines correspond to zero level.

thickness and from the slits. The frequencies of the coupled modes are given by

$$\omega_{\pm}^2 = \tfrac{1}{2}(\omega_{\mathrm{a}}^2 + \omega_{\mathrm{d}}^2 \pm \sqrt{(\omega_{\mathrm{a}}^2 - \omega_{\mathrm{d}}^2)^2 + 4\eta_1\eta_2}), \tag{5}$$

where ω_{d} and ω_{a} are the eigenfrequencies of the oscillators, i.e. the frequencies of the metal/magnetic–dielectric and air/metal SPPs, respectively, and $\eta_{1,2}$ are the coupling coefficients depending on the grating parameters. If ω_{d} and ω_{a} differ significantly so that $|\omega_{\mathrm{a}}^2 - \omega_{\mathrm{d}}^2| \gg \sqrt{\eta_1\eta_2}$, then the SPPs at the two interfaces exist almost independently of each other and $\omega_{\pm} \approx \omega_{\mathrm{d}}, \omega_{\mathrm{a}}$. As ω_{d} and ω_{a} approach each other, the coupling between the SPP modes increases and their frequencies $\omega_{\pm}$ become dependent on both ω_{d} and ω_{a}. The resonance frequency ω_d depends on the magnetization according to equation (4), leading to a dependence of the frequencies of both modes defined by equation (5) on the magnetization. That is why, in the vicinity of the crossing of the dispersion curves for the air/metal and metal/magnetic–dielectric SPPs, the TMOKE is enhanced at either of the modes. As will be discussed further, this

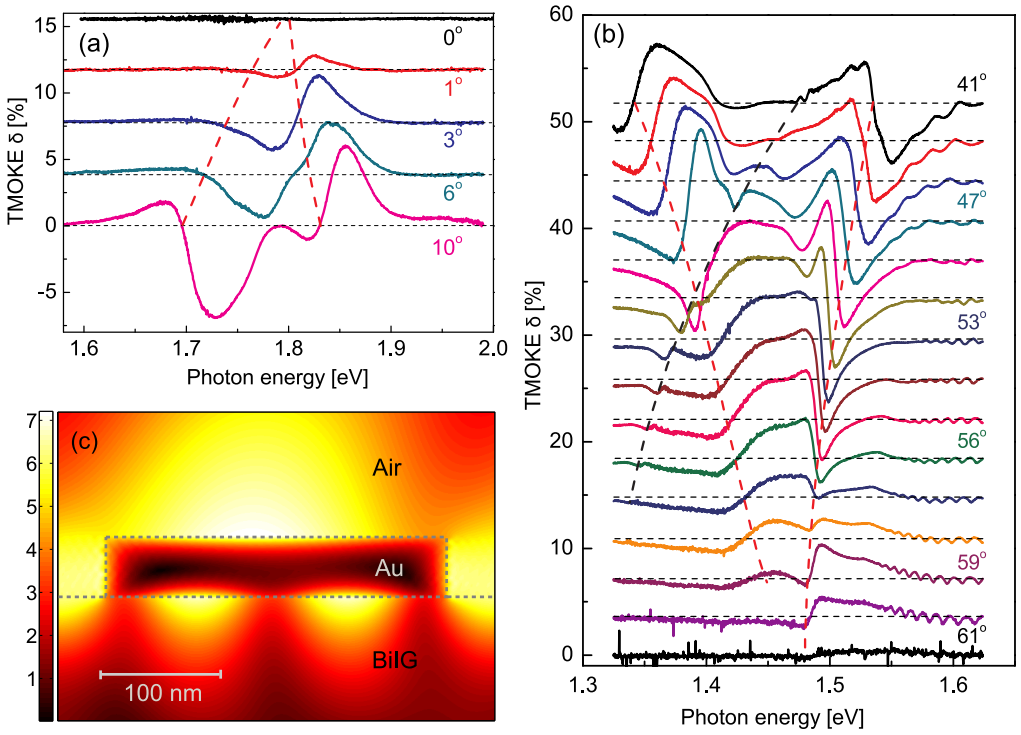

Figure 5. The TMOKE measured in transmission with sample 2 at incidence angles (a) close to $k = 0$ (from 0° to 10°) and (b) from 41° to 61°, i.e. close to the edge of the first Brillouin zone. The dashed lines are guides to the eye representing the shift of the TMOKE features. Surprisingly, close to the intersection of the SPP dispersions, the curves show features whose shift can be attributed not only to the Au/BIG magneto-plasmon (red dashed lines) but also to the Au/air SPP (black dashed line, compare figures 4(a) and (b)). At both $k = 0$ as well as at the 1.BZ edge, the TMOKE amplitude is zero due to symmetry considerations. The contour plot in (c) shows the calculated near field spatial distributions of the square of the absolute value of the magnetic field $|H|^2$ at $\theta = 49°$ and photon energy 1.38 eV.

enhancement is the result of the magnetization induced shift of the plasmonic resonance rather than of vanishing transmittance.

The maximum amplitude of the TMOKE in this sample is obtained at 1.4 eV and 47°, i.e. in the vicinity of the SPP anti-crossing, reaching 8.5%. Additionally, in the same range of angles, enhanced optical transmission is observed, which exceeds 25%. This value, which is considerably higher than would be expected from direct transmission through the grating slits, involves tunneling of the air/metal SPP to the metal/magnetic–dielectric interface due to the finite grating depths and subsequent radiative scattering into the forward direction [43].

Figure 5(c) gives an example of the optical magnetic field distribution $|H|^2$ near the grating (gray box) in the vicinity of the SPP anti-crossing ($\theta = 49°$ and photon energy 1.38 eV). It supports the above reasoning by showing simultaneous excitation of the air/metal and metal/magnetic–dielectric SPPs.

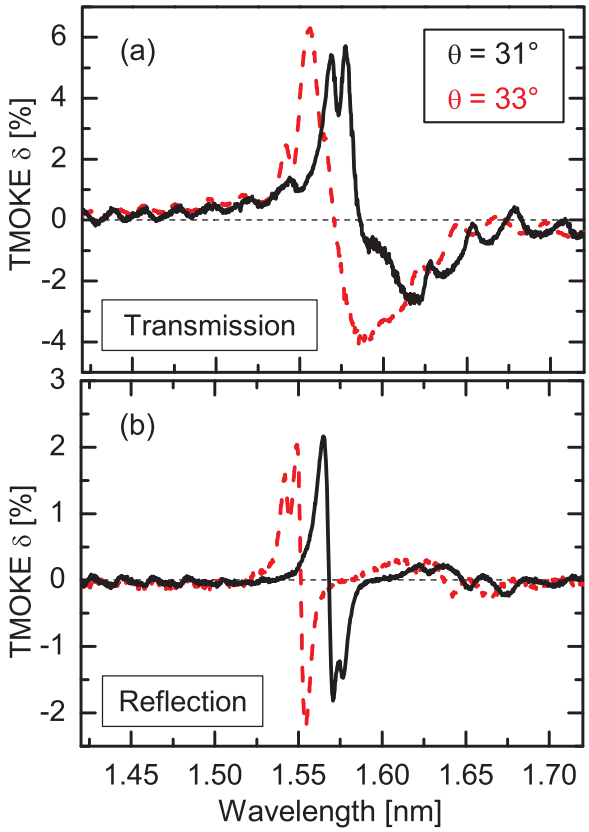

Figure 6. The TMOKE signals of sample 2 for the incidence angles $\theta = 31^\circ$ (solid) and $\theta = 33^\circ$ (dashed) measured in (a) transmission and (b) reflection.

5. Transmission versus reflection

Although the enhancing mechanism of the TMOKE by SPPs has already been elucidated (see section 3 and [8]), the observed phenomena can be unambiguously identified as surface effects through measurements of the reflectivity from the gold side of the MPCs. This way, contributions from the bulk BIG can be excluded.

Figure 6 gives a comparison of the TMOKE in transmission (figure 6(a)) and in reflection from the top gold grating (figure 6(b)) at incidence angles of 31° and 33°. In full accord and with our expectations, the effect is observed in both reflection and transmission geometries, resembling each other in shape and position. The magnitude is reduced in reflection by a factor of 3, which can be explained as follows. The value of TMOKE is in first order of the magnetization proportional to the derivative of $I(E)$ with respect to the photon energy, i.e. $\delta(E, M) = a(\partial I(E)/\partial E)M/I(E)$ with a proportionality constant a (see e.g. [8]). In the vicinity of a Fano resonance, $I(E)$ is given by equation (2), where $I_r(E)$ can be expressed by a normalized function $S(E)$ and an amplitude I_0 in the following way $I_r(E) = I_0 S(E)$. This leads to

$$\delta(E, M) = \frac{a I_0 M(\partial S(E)/\partial E)}{I_{nr} + I_0 S(E)}. \tag{6}$$

In transmission spectra, I_{nr} is usually much smaller than I_0, which makes $\delta_T(E, M)$ almost independent of the transmitted light intensity: $\delta_T(E, M) = aM(\partial S(E)/\partial E)/S(E)$. This proves that the enhancement of the TMOKE is due to the magnetization induced shift of the Fano resonance rather than due to low values of the transmitted light intensity. On the other hand, the contribution of I_{nr} in reflection is more pronounced and since it enters in equation (6) in the denominator it diminishes the TMOKE value.

Figure 6(b) also reveals a decreased linewidth as compared to the transmission signals, which is due to the different Fano resonance shapes of transmittance and reflectance (see figures 4(c) and (d)). The curves are superimposed by high-frequency oscillations with a period of about 50 meV originating from Fabry–Perot interferences inside the magnetic film of thickness $h_d = 5.095\,\mu$m. These oscillations are weaker in reflection with an amplitude at least one order of magnitude smaller than the TMOKE peaks. Consequently, the part of the reflected light that penetrates the bulk film as well as a possible contribution to the signal can be neglected.

6. Conclusions

The results illustrate the importance of MPCs for applications involving the TMOKE in either transmission or reflection geometries. It has been shown that the magnitude of the effect can reach up to 10% and even higher depending on the bismuth substitution level of the magneto-optically active layer. At the same time, these magnitudes can be achieved at low magnetic fields and in nanometer scale volumes due to the small saturation magnetic field ($\leqslant 100$ mT, see figure 3) and the high confinement of the SPPs to the film surfaces. Since the described phenomena are localized to few hundreds of nanometers in the direction perpendicular to the interfaces, corresponding to the skin depth of the SPPs in the adjacent materials, rather than being bulk phenomena, material costs can be largely reduced leading the way to miniaturized magneto-optical applications, such as all-optical switches and modulators. Furthermore, the results demonstrate that the effect can be arbitrarily tuned to energies, which are easily accessible by a broad range of commercially available laser systems, by a simple rotation of the sample and/or by appropriate design of the grating parameters. Despite the presumably advantageous transmission geometry for future applications, the reflection geometry provides one additional degree of freedom. Further potential is implied by the optical switching of the magnetization by means of the inverse Faraday effect instead of using external fields, which promises to accelerate switching times into the ultrafast regime.

Acknowledgments

This work was supported by the Deutsche Forschungsgemeinschaft through grant number AK-40/7-1, the Russian Foundation for Basic Research (project numbers 12-02-33100, 12-02-31298, 13-02-01122, 13-02-91334, 11-02-00681) and the Russian Federal Targeted Program ‘Scientific and Scientific-Pedagogical Personnel of the Innovative Russia’. VIB and ANK additionally acknowledge support by an Alexander von Humboldt Foundation personal grant and Russian Presidential Fellowship (number SP-124.2012.5), respectively.

References

[1] Inoue M, Khanikaev A and Baryshev A 2009 Nano-magnetophotonics *Nanoscale Magnetic Materials and Applications* ed J Ping Liu, E Fullerton, O Gutfleisch and D J Sellmyer (Boston, MA: Springer) pp 627–59

[2] Zvezdin A K and Kotov V A 1997 *Modern Magnetooptics and Magnetooptical Materials* 1st edn (London: Taylor and Francis)

[3] Kirilyuk A, Kimel A V and Rasing T 2010 Ultrafast optical manipulation of magnetic order *Rev. Mod. Phys.* **82** 2731–84

[4] Mansuripur M 1998 *The Physical Principles of Magneto-Optical Recording* 2nd edn (Cambridge: Cambridge University Press)

[5] Grunin A A, Zhdanov A G, Ezhov A A, Ganshina E A and Fedyanin A A 2010 Surface-plasmon-induced enhancement of magneto-optical kerr effect in all-nickel subwavelength nanogratings *Appl. Phys. Lett.* **97** 261908

[6] Clavero C, Yang K, Skuza J R and Lukaszew R A 2010 Magnetic-field modulation of surface plasmon polaritons on gratings *Opt. Lett.* **35** 1557–9

[7] Torrado J F, González-Díaz J B, González M U, García-Martín A and Armelles G 2010 Magneto-optical effects in interacting localized and propagating surface plasmon modes *Opt. Express* **18** 15635–42

[8] Belotelov V I, Akimov I A, Pohl M, Kotov V A, Kasture S, Vengurlekar A S, Venu Gopal A, Yakovlev D R, Zvezdin A K and Bayer M 2011 Enhanced magneto-optical effects in magnetoplasmonic crystals *Nature Nanotechnol.* **6** 370–6

[9] Belotelov V I, Bykov D A, Doskolovich L L, Kalish A N and Zvezdin A K 2009 Extraordinary transmission and giant magneto-optical transverse kerr effect in plasmonic nanostructured films *J. Opt. Soc. Am.* B **26** 1594–8

[10] Belotelov V I, Bykov D A, Doskolovich L L, Kalish A N and Zvezdin A K 2010 Giant transversal kerr effect in magneto-plasmonic heterostructures: the scattering-matrix method *J. Exp. Theor. Phys.* **110** 816–24

[11] Maier S A 2007 *Plasmonics: Fundamentals and Applications* 2007 edn (Berlin: Springer)

[12] Temnov V V, Armelles G, Woggon U, Guzatov D, Cebollada A, Garcia-Martin A, Garcia-Martin J M, Thomay T, Leitenstorfer A and Bratschitsch R 2010 Active magneto-plasmonics in hybrid metal–ferromagnet structures *Nature Photon.* **4** 107–11

[13] Temnov V V 2012 Ultrafast acousto-magneto-plasmonics *Nature Photon.* **6** 728–36

[14] Akimov I A *et al* 2012 Hybrid structures of magnetic semiconductors and plasmonic crystals: a novel concept for magneto-optical devices [invited] *J. Opt. Soc. Am.* B **29** A103–18

[15] Belotelov V I, Doskolovich L L and Zvezdin A K 2007 Extraordinary magneto-optical effects and transmission through metal–dielectric plasmonic systems *Phys. Rev. Lett.* **98** 077401

[16] Fang K, Yu Z, Liu V and Fan S 2011 Ultracompact nonreciprocal optical isolator based on guided resonance in a magneto-optical photonic crystal slab *Opt. Lett.* **36** 4254–6

[17] Bi L, Hu J, Jiang P, Kim D H, Dionne G F, Kimerling L C and Ross C A 2011 On-chip optical isolation in monolithically integrated non-reciprocal optical resonators *Nature Photon.* **5** 758–62

[18] Sapozhnikov M V, Gusev S A, Troitskii B B and Khokhlova L V 2011 Optical and magneto-optical resonances in nanocorrugated ferromagnetic films *Opt. Lett.* **36** 4197–9

[19] Ctistis G, Papaioannou E, Patoka P, Gutek J, Fumagalli P and Giersig M 2009 Optical and magnetic properties of hexagonal arrays of subwavelength holes in optically thin cobalt films *Nano Lett.* **9** 1–6

[20] Belotelov V I and Zvezdin A K 2006 Magnetooptics and extraordinary transmission of the perforated metallic films magnetized in polar geometry *J. Magn. Magn. Mater.* **300** e260–3

[21] Newman D M, Wears M L, Matelon R J and Hooper I R 2008 Magneto-optic behaviour in the presence of surface plasmons *J. Phys.: Condens. Matter* **20** 345230

[22] Armelles G, Cebollada A, García-Martín A, García-Martín J M, González M U, González-Díaz J B, Ferreiro-Vila E and Torrado J F 2009 Magnetoplasmonic nanostructures: systems supporting both plasmonic and magnetic properties *J. Opt. A: Pure Appl. Opt.* **11** 114023

[23] Manera M G *et al* 2011 Enhanced gas sensing performance of TiO_2 functionalized magneto-optical SPR sensors *J. Mater. Chem.* **21** 16049–56
[24] Banthí J C, Meneses-Rodríguez D, García F, González M U, García-Martín A, Cebollada A and Armelles G 2012 High magneto-optical activity and low optical losses in metal-dielectric Au/Co/Au–SiO_2 magnetoplasmonic nanodisks *Adv. Mater.* **24** OP36–41
[25] Davoyan A R, Mahmoud A M and Engheta N 2013 Optical isolation with epsilon-near-zero metamaterials *Opt. Express* **21** 3279–86
[26] Chin J Y, Steinle T, Wehlus T, Dregely D, Weiss T, Belotelov V I, Stritzker B and Giessen H 2013 Nonreciprocal plasmonics enables giant enhancement of thin-film faraday rotation *Nature Commun.* **4** 1599
[27] Khanikaev A B, Hossein S Mousavi, Shvets G and Kivshar Y S 2010 One-way extraordinary optical transmission and nonreciprocal spoof plasmons *Phys. Rev. Lett.* **105** 126804
[28] Strelniker Y M and Bergman D J 1999 Optical transmission through metal films with a subwavelength hole array in the presence of a magnetic field *Phys. Rev.* B **59** R12763–6
[29] Strelniker Y M and Bergman D J 2008 Transmittance and transparency of subwavelength-perforated conducting films in the presence of a magnetic field *Phys. Rev.* B **77** 205113
[30] Armelles G, Cebollada A, García-Martín A and González M U 2013 Magnetoplasmonics: combining magnetic and plasmonic functionalities *Adv. Opt. Mater.* **1** 10–35
[31] Ferguson P, Stafsudd O and Wallis R 1977 Surface magnetoplasma waves in nickel *Physica* B+C **86** 1403–5
[32] Burke J J, Stegeman G I and Tamir T 1986 Surface-polariton-like waves guided by thin, lossy metal films *Phys. Rev.* B **33** 5186–201
[33] Aers G C and Boardman A D 1978 The theory of semiconductor magnetoplasmon-polariton surface modes: Voigt geometry *J. Phys. C: Solid State Phys.* **11** 945–59
[34] Kushwaha M S 2001 Plasmons and magnetoplasmons in semiconductor heterostructures *Surf. Sci. Rep.* **41** 1–416
[35] Miroshnichenko A E, Flach S and Kivshar Y S 2010 Fano resonances in nanoscale structures *Rev. Mod. Phys.* **82** 2257–98
[36] Wood R W 1935 Anomalous diffraction gratings *Phys. Rev.* **48** 928–36
[37] Grunin A A, Sapoletova N A, Napolskii K S, Eliseev A A and Fedyanin A A 2012 Magnetoplasmonic nanostructures based on nickel inverse opal slabs *J. Appl. Phys.* **111** 07A948
[38] González-Diáz J B, Sepúlveda B, Garciá-Martín A and Armelles G 2010 Cobalt dependence of the magneto-optical response in magnetoplasmonic nanodisks *Appl. Phys. Lett.* **97** 043114
[39] González-Díaz J B, García-Martín A, Armelles G, García-Martín J M, Clavero C, Cebollada A, Lukaszew R A, Skuza J R, Kumah D P and Clarke R 2007 Surface-magnetoplasmon nonreciprocity effects in noble-metal/ferromagnetic heterostructures *Phys. Rev.* B **76** 153402
[40] Armelles G, González-Díaz J B, García-Martín A, García-Martín J M, Cebollada A, González M U, Acimovic S, Cesario J, Quidant R and Badenes G 2008 Localized surface plasmon resonance effects on the magneto-optical activity of continuous Au/Co/Au trilayers *Opt. Express* **16** 16104–12
[41] Torrado J F, González-Díaz J B, Armelles G, García-Martín A, Altube A, López-García M, Galisteo-López J F, Blanco A and López C 2011 Tunable magneto-photonic response of nickel nanostructures *Appl. Phys. Lett.* **99** 193109
[42] Hibiya T, Morishige Y and Nakashima J 1985 Growth and characterization of liquid-phase epitaxial bi-substituted iron garnet films for magneto-optic application *Japan. J. Appl. Phys.* **24** 1316–9
[43] Genet C and Ebbesen T W 2007 Light in tiny holes *Nature* **445** 39–46